Engineering Transactions, **72**(1): 15–38, 2024, doi: 10.24423/EngTrans.3074.2024
Institute of Fundamental Technological Research Polish Academy of Sciences (IPPT PAN)
Université de Lorraine • Poznan University of Technology

Research Paper

Lengthwise Crack Study of a Beam with Non-Linear Creep

Victor Iliev RIZOV

Department of Technical Mechanics
University of Architecture, Civil Engineering and Geodesy
1 Chr. Smirnensky Blvd., 1046 – Sofia, Bulgaria; e-mail: v_rizov_fhe@uacg.bg

An analytical study of the strain energy release rate for an inhomogeneous beam structure with a lengthwise crack subjected to non-linear creep is developed. The beam is inhomogeneous along its length. Two cases are analysed (material with identical creep behaviour in tension and compression, and material with asymmetrical creep behaviour). Since the stress cannot be determined explicitly from the non-linear stress-strain-time relationship, an approach for obtaining of time-dependent solutions of the strain energy release rate is developed by expressing the z-coordinate as a function of the stress. The analysis indicates that the asymmetrical creep behaviour leads to an increase in the strain energy release rate.

Keywords: beam structure; non-linear creep; lengthwise crack.

1. Introduction

Due to their superior mechanical properties, such as high strength-to-weight and stiffness-to-weight ratios and good processability, structural members and components made of continuously inhomogeneous functionally graded materials are widely used in various engineering applications in modern technology [1–7]. The effects of inhomogeneity on stresses distributions in functionally graded discs were analysed by applying the theory of elasticity in [1–3]. An efficient method for the thermo-elastic analysis of functionally graded rotating disks of variable thickness was developed in [3]. A functionally graded beam under combined loads was investigated analytically in [4]. A method applicable for a vast class of functionally graded and variable thickness beams was presented, and A study of the effect of non-homogenous coefficient on the rotation and deflection of the beam was carried out [4].

Functionally graded beams resting on a nonlinear foundation were investigated in [5]. A method that can be applied on both linear and nonlinear foundations was developed [5]. An analytical solution of a curved beam made of functionally graded materials was derived in [6], where the influence of material non-homogeneity on the radial distribution of circumferential stress was

studied. Nonlinear static deflections of functionally graded porous beams under thermal effect were investigated in [7], where different porosity models were applied and discussed. The nonlinear displacements of laminated composite beams were studied under non-uniform temperature in [8]. Post-buckling analysis of a functionally graded beam under hygro-thermal effect was performed assuming a power-law variation of material properties along the beam thickness [9]. Furthermore, design, modelling, processing and evaluation of functionally graded materials as well as their applications were described comprehensively in [10]. An introduction to the functionally graded material can be found in [11], where a brief description of different functionally graded materials and their presence in nature was presented. A critical review of the functionally graded materials and their use in various areas can be found in [12]. Additionally, a review of modelling studies related to functionally graded materials was presented in [13]. Lastly, processing methods of functionally graded materials were discussed in [14].

Functionally graded materials usually have a layered structure [8–14]. Therefore, they are prone to the development of lengthwise cracks between layers. In fact, lengthwise fractures are among the most common failure modes of beam structures made of continuously inhomogeneous engineering materials. The lengthwise cracks diminish the strength and load-bearing capacity, compromise the stability and increase the deformability of structural members.

Lengthwise fracture of inhomogeneous beams with a layered structure was analysed in [15], where solutions for the strain energy release rate were obtained. For this purpose, linear-elastic fracture mechanics was applied since the layers exhibited the linear-elastic behaviour [15]. Additionally, layered beam structural members with linear-elastic behaviour were investigated in [16], with solutions of the strain energy release rate for lengthwise cracks derived by using linear-elastic fracture mechanics. Fracture in beams made of continuously inhomogeneous (functionally graded) materials was analysed theoretically in [17]. The basic hypothesis used in [17] was that the layers exhibit linear-elastic behaviour. Various works on the fracture behaviour of materials with a graded structure were reviewed in [18], along with considerations of numerous applications of the linear-elastic fracture mechanics]. The study also included analyses of cracks in materials with graded structure under cyclic fatigue loading conditions [18]. Furthermore, a theoretical study of continuously inhomogeneous (functionally graded) beams with cracks was developed in [19] for the case of linear-elastic behaviour of the material, where exponential distributions of the material properties in the beam structure were assumed. It seems that existing works on lengthwise cracks in continuously inhomogeneous beam structures deal mainly with layers exhibiting linear-elastic behaviour.

However, one of the factors influencing the lengthwise fracture behaviour is creep. This factor deserves a thorough study because engineering structures

oftentimes are under external loads that do not change with time. These loads usually induce material creep.

Therefore, the main objective of the present paper is to develop an analytical study of the strain energy release rate with taking into account non-linear creep for a lengthwise crack in a continuously inhomogeneous beam configuration in the longitudinal direction. In order to accomplish this, a time-dependent solution of the complementary strain energy cumulated in the beam is derived by using a non-linear stress-strain-time relationship (two cases are considered – a material with identical creep behaviour in tension and compression and a material with asymmetrical creep behaviour in tension and compression). Then, time-dependent solutions of the strain energy release rate are obtained by differentiating the time-dependent complementary strain energy with respect to the crack area. In order to verify these solutions, the time-dependent strain energy release rate is also derived by considering the energy balance. The solutions derived are applied to investigate the change of the strain energy release rate with time due to non-linear creep behaviour. Additionally, the influence of asymmetrical creep behaviour of the material in tension and compression on the strain energy release rate is evaluated. It should be underlined that the key novelty in the present paper is that non-linear creep is taken into account (distinguishing it from previous papers that concentrated on lengthwise fracture analyses in continuously inhomogeneous beam configurations with linear creep behaviour [20, 21]). It should also be specified that the present analysis is carried out for small strains.

2. Beam with identical creep behaviour in tension and compression

A simply supported inhomogeneous beam configuration with one lengthwise crack, as shown schematically in Fig. 1, is under consideration in this paper. The length of the beam is denoted by l. The beam cross-section is a rectangle of width b and thickness h. A vertical notch of depth h_2 is cut out in the lower surface of the beam at a distance l_1 from the left-hand end of the beam. The notch in the beam in Fig. 1 is needed to induce conditions for lengthwise cracking. However, in real beam specimens the presence of such a notch is not obligatory. For instance, lengthwise cracking can occur at the end sections of the beam structure. In fact, the beam configuration considered in the paper (Fig. 1) illustrates the way for application of the approach to treat lengthwise cracks in functionally graded beams exhibiting non-linear creep behaviour. A lengthwise crack of length a is located in the beam portion B_2B_3, as shown in Fig. 1. The upper and lower crack arms have different thicknesses, denoted by h_1 and h_2, respectively. The beam is subjected to three-point bending by a vertical force F applied at the mid-span. It is obvious that the lower crack arm is free of stresses

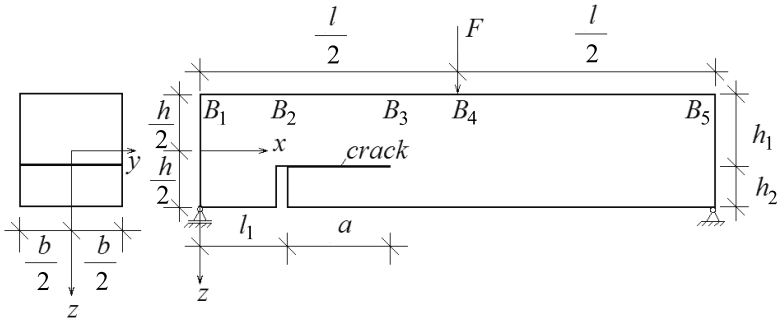

FIG. 1. Geometry and loading of a beam structure with a lengthwise crack.

(Fig. 1). The beam under consideration exhibits non-linear creep behaviour, addressed by using the following non-linear stress-strain-time relationship [22]:

$$\varepsilon = A_0 \sinh(\beta_0 \sigma) + A^n t^n \sinh(\beta \sigma), \tag{2.1}$$

where ε is the strain, σ is the normal stress, t is the time, A_0, β_0, A, β, and n are material constants. It should be noted that the first term on the right-hand side of formula (2.1) describes the instantaneous strain, while the creep strain is described by the second term on the right-hand side of (2.1). It is evident from (2.1) that both the instantaneous and the creep strains depend non-linearly on stress. Non-linear stress-strain-time relationship, Eq. (2.1), illustrates the approach for application of the analysis. Other non-linear stress-strain-time relationships can also be used depending on the particular problem under consideration. It should also be noted that at time = infinity, the creep strain approaches infinity according to Eq. (2.1). However, it should be noted that the present analysis is carried out for small strains, i.e., the case 'time = infinity' is beyond the scope of the paper (actually, at time = infinity the beam would fail as a result of an unlimited growth of the creep strains). It should also be noted that the present study assumes that the crack will begin to propagate long before the failure of the beam as a result of the unlimited growth of creep strains.

Due to material inhomogeneity, A_0 and A vary continuously along the beam length according to the following laws:

$$A_0 = A_{0KR} e^{\varphi_0 \frac{x}{l}}, \qquad A = A_{KR} e^{\varphi \frac{x}{l}}, \tag{2.2}$$

where A_{0KR} and A_{KR} are the values of A_0 and A at the left-hand end of the beam, φ_0 and φ are material constants, x is the position along the centroidal axis of the beam (Fig. 1). The application of Eq. (2.2) is based on the fact that the exponential laws are frequently used to describe the distribution of properties in continuously inhomogeneous structural members.

The strain energy release rate for the lengthwise crack shown in Fig. 1 is obtained by using the complementary strain energy. For this purpose, the strain energy release rate G is written as:

$$G = \frac{1}{b}\frac{\mathrm{d}U^*}{\mathrm{d}a}, \tag{2.3}$$

where U^* is the complementary strain energy, and $\mathrm{d}a$ is an elementary increase of crack length. The complementary strain energy involved in Eq. (2.3) is found as:

$$U^* = U_1^* + U_2^*, \tag{2.4}$$

where U_1^* and U_2^* are the complementary strain energies cumulated in the upper crack arm and the beam portion B_3B_4, respectively. It should be mentioned that the complementary strain energy in the lower crack arm is zero since this crack arm is free of stresses. It should also be mentioned that the complementary strain energies cumulated in beam portions B_1B_2 and B_4B_5 are not included in formula (2.4) since these energies do not depend on a.

The complementary strain energy in the upper crack arm is obtained by integrating the complementary strain energy density u_{01}^* in the volume of the upper crack arm:

$$U_1^* = b \int_{l_1}^{l_1+a} \int_{-\frac{h_1}{2}}^{\frac{h_1}{2}} u_{01}^* \,\mathrm{d}x\,\mathrm{d}z_1, \tag{2.5}$$

where z_1 is the vertical centric axis of the cross-section of the upper crack arm. The complementary strain energy density is numerically equal to the area that supplements the area enclosed by the stress-strain curve to form a rectangle. Therefore, the complementary strain energy density is written as:

$$u_{01}^* = \sigma\varepsilon - u_{01}, \tag{2.6}$$

where u_{01} is the strain energy density. As commonly known, the strain energy density is equal to the area enclosed by the stress-strain curve. Thus, u_{01} is expressed as:

$$u_{01} = \int \sigma \,\mathrm{d}\varepsilon. \tag{2.7}$$

From formula (2.1), $\mathrm{d}\varepsilon$ is derived as:

$$\mathrm{d}\varepsilon = \left[A_0\beta_0 \cosh(\beta_0\sigma) + A^n\beta t^n \cosh(\beta\sigma)\right]\mathrm{d}\sigma. \tag{2.8}$$

By substituting (2.8) into (2.7), one obtains:

(2.9)
$$u_{01} = A_0 \left[\sigma \sinh(\beta_0 \sigma) - \frac{1}{\beta_0} \cosh(\beta_0 \sigma)\right] + A^n t^n \left[\sigma \sinh(\beta \sigma) - \frac{1}{\beta} \cosh(\beta \sigma)\right].$$

By combining (2.1), (2.6) and (2.9), one derives

$$u_{01}^* = \frac{A_0}{\beta_0} \cosh(\beta_0 \sigma) + \frac{A^n}{\beta} t^n \cosh(\beta \sigma). \tag{2.10}$$

In order to verify formula (2.10), the complementary strain energy density is written as:

$$u_{01}^* = \int \varepsilon \, \mathrm{d}\sigma. \tag{2.11}$$

By substituting (2.1) into (2.11), one obtains an expression for the complementary strain energy density that exactly matches (2.10).

The complementary strain energy density has to be presented as a function of z_1 in order to perform the integration in (2.5). For this purpose, the stress-strain-time relationship (2.1) is used. In the present paper, the distribution of the strains involved in (2.1) is treated by applying Bernoulli's hypothesis for plane sections since beams of high length-to-thickness ratio are under consideration. Therefore, the distribution of z_1 along the thickness of the cross-section of the upper crack arm is expressed as:

$$\varepsilon = \kappa_1 z_1, \tag{2.12}$$

where κ_1 is the curvature of the upper crack arm. By substituting (2.12) into (2.1), one obtains:

$$\kappa_1 z_1 = A_0 \sinh(\beta_0 \sigma) + A^n t^n \sinh(\beta \sigma). \tag{2.13}$$

The stress σ cannot be determined explicitly from Eq. (2.13). Therefore, in order to facilitate the integration in (2.5), z_1 and dz_1 are presented as functions of the stress. By using (2.13), z_1 is obtained as:

$$z_1 = \frac{1}{\kappa_1} \left[A_0 \sinh(\beta_0 \sigma) + A^n t^n \sinh(\beta \sigma)\right]. \tag{2.14}$$

From formula (2.14), one derives

$$\mathrm{d}z_1 = \frac{1}{\kappa_1} \left[A_0 \beta_0 \cosh(\beta_0 \sigma) + A^n \beta t^n \cosh(\beta \sigma)\right] \mathrm{d}\sigma. \tag{2.15}$$

The curvature involved in (2.15) is determined in the following way. First, the equation for the equilibrium of the cross-section of the upper crack arm is written as:

$$M = b \int_{-\frac{h_1}{2}}^{\frac{h_1}{2}} \sigma z_1 \, \mathrm{d}z_1, \tag{2.16}$$

where the bending moment is obtained as (Fig. 1):

$$M = \frac{F}{2} x. \tag{2.17}$$

Then by substituting (2.14) and (2.15) into (2.16), and integrating in the boundaries from $-\sigma_{sr}$ to σ_{sr}, one derives

$$\begin{aligned} M = {} & A_0^2 \frac{b}{2\kappa_1^2} \left[\sigma_{sr} \cosh\left(2\beta_0 \sigma_{sr}\right) - \frac{1}{2\beta_0} \sinh\left(2\beta_0 \sigma_{sr}\right) \right] \\ & + A^n A_0 t^n \frac{b}{\kappa_1^2} \left\{ \sigma_{sr} \cosh\left[\left(\beta_0 + \beta\right) \sigma_{sr}\right] - \frac{1}{\beta + \beta_0} \sinh\left[\left(\beta_0 + \beta\right) \sigma_{sr}\right] \right\} \\ & + A^n A_0 \beta t^n \frac{b}{\kappa_1^2} \left\{ \frac{1}{\beta_0 - \beta} \sigma_{sr} \cosh\left[\left(\beta_0 - \beta\right) \sigma_{sr}\right] - \frac{1}{\left(\beta_0 - \beta\right)^2} \sinh\left[\left(\beta_0 - \beta\right) \sigma_{sr}\right] \right\} \\ & + A^n A_0 \beta_0 t^n \frac{b}{\kappa_1^2} \left\{ \frac{1}{\beta - \beta_0} \sigma_{sr} \cosh\left[\left(\beta - \beta_0\right) \sigma_{sr}\right] - \frac{1}{\left(\beta - \beta_0\right)^2} \sinh\left[\left(\beta - \beta_0\right) \sigma_{sr}\right] \right\} \\ & + A^{2n} t^{2n} \frac{b}{2\kappa_1^2} \left[\sigma_{sr} \cosh\left(2\beta \sigma_{sr}\right) - \frac{1}{2\beta} \sinh\left(2\beta \sigma_{sr}\right) \right], \end{aligned} \tag{2.18}$$

where $-\sigma_{sr}$ and σ_{sr} are the normal stresses at the upper and lower surfaces of the upper crack arm, respectively. There are two unknowns κ_1 and σ_{sr} in Eq. (2.18). Further, one equation is written by substituting $z_1 = h_1/2$ and $\sigma = \sigma_{sr}$ into formula (2.13)

$$\kappa_1 \frac{h_1}{2} = A_0 \sinh\left(\beta_0 \sigma_{sr}\right) + A^n t^n \sinh\left(\beta \sigma_{sr}\right). \tag{2.19}$$

Equations (2.18) and (2.19) are solved with respect to κ_1 and σ_{sr} by using the MATLAB computer program.

The complementary strain energy cumulated in the beam portion B_3B_4 is written as:

$$U_2^* = b \int_{l_1+a}^{\frac{l}{2}} \int_{-\frac{h}{2}}^{\frac{h}{2}} u_{02}^* \, \mathrm{d}x \, \mathrm{d}z_2, \tag{2.20}$$

where u_{02}^* is the complementary strain energy density, and z_2 is the vertical centric axis of the cross-section of the beam portion B_3B_4. The complementary strain energy density is found using (2.10). The quantity $\mathrm{d}z_2$ is obtained by applying formula (2.15). For this purpose, κ_1 is replaced with the curvature κ_2 of the beam portion B_3B_4:

$$\mathrm{d}z_2 = \frac{1}{\kappa_2}\left[A_0\beta_0\cosh(\beta_0\sigma) + A^n\beta t^n\cosh(\beta\sigma)\right]\mathrm{d}\sigma. \tag{2.21}$$

The curvature κ_2 and the normal stress σ_{uc} at the lower surface of the beam in the portion B_3B_4 are derived by using Eqs. (2.18) and (2.19). For this purpose, κ_1, h_1 and σ_{sr} are replaced, respectively, with κ_2, h_2 and σ_{uc}, and then Eqs. (2.18) and (2.19) are solved with respect to κ_2 and σ_{uc} using the MATLAB computer program.

By substituting of (2.4), (2.5) and (2.20) into (2.3) and expressing the boundaries of integration through σ_{sr} and σ_{uc}, one derives the following expression for the strain energy release rate:

$$G = \int\limits_{-\sigma_{sr}}^{\sigma_{sr}} u_{01}^*\,\mathrm{d}z_1 - \int\limits_{-\sigma_{uc}}^{\sigma_{uc}} u_{02}^*\,\mathrm{d}z_2, \tag{2.22}$$

where $\mathrm{d}z_1$ and $\mathrm{d}z_2$ are found by using (2.15) and (2.21), respectively. It should be noted here that κ_1, σ_{sr}, κ_2 and σ_{uc} are obtained by Eqs. (2.18) and (2.19) at $x = l_1 + a$. The integration in (2.22) is carried out using the MATLAB computer program.

In order to verify solution (2.22), the strain energy release rate is also derived by analysing the balance of the energy. For this purpose, a small increase δa of the length of the crack is given. The balance of the energy is expressed as:

$$F\delta w = \frac{\partial U}{\partial a}\delta a + Gb\delta a, \tag{2.23}$$

where w is the vertical displacement of the application point B_4 of the external force, U is the strain energy. From (2.23), the strain energy release rate is derived as:

$$G = \frac{F}{b}\frac{\partial w}{\partial a} - \frac{1}{b}\frac{\partial U}{\partial a}. \tag{2.24}$$

The integrals of Maxwell-Mohr are applied to determine w. For this purpose, the integrals are written as (Fig. 1):

$$w = \int_0^{l_1} \kappa_{B_1B_2} M_1(x)\,\mathrm{d}x + \int_{l_1}^{l_1+a} \kappa_1 M_1(x)\,\mathrm{d}x + \int_{l_1+a_1}^{\frac{l}{2}} \kappa_2 M_1(x)\,\mathrm{d}x + \int_{\frac{l}{2}}^{l} \kappa_{B_3B_5} M_2(x)\,\mathrm{d}x, \tag{2.25}$$

where $\kappa_{B_1B_2}$ and $\kappa_{B_3B_5}$ are, respectively, the curvatures in beam portions B_1B_2 and B_4B_5, and $M_1(x)$ and $M_2(x)$ are the bending moments induced by the unit loading for obtaining w in beam portions B_1B_4 and B_4B_5, respectively. Since

$$M_1(x) = \frac{x}{2} \tag{2.26}$$

and

$$M_2(x) = \frac{l}{2} - \frac{x}{2}, \tag{2.27}$$

the integrals (2.25) take the following form:

$$w = \int_0^{l_1} \kappa_{B_1B_2} \frac{x}{2}\,\mathrm{d}x + \int_{l_1}^{l_1+a} \kappa_1 \frac{x}{2}\,\mathrm{d}x + \int_{l_1+a_1}^{\frac{l}{2}} \kappa_2 \frac{x}{2}\,\mathrm{d}x + \int_{\frac{l}{2}}^{l} \kappa_{B_3B_5} \left(\frac{l}{2} - \frac{x}{2}\right)\,\mathrm{d}x. \tag{2.28}$$

In view of the fact that in formula (2.24) w is differentiated with respect to the crack length a, it is not necessary to determine the curvatures $\kappa_{B_1B_2}$ and $\kappa_{B_3B_5}$, since the first and the last terms in the right-hand side of (2.28) do not depend on a.

The strain energy involved in (2.24) is written as:

$$U = U_1 + U_2, \tag{2.29}$$

where U_1 and U_2 are, respectively, the strain energies in the upper crack arm and in the beam portion B_3B_4. The strain energy in the lower crack arm is zero since this crack arm is free of stresses. The strain energies in beam portions B_1B_2 and B_4B_5 are not involved in (2.29) since these energies do not depend on a.

The strain energy in the upper crack is obtained by applying formula (2.5). For this purpose, u_{01}^* is replaced with the strain energy density u_{01}. Formula (2.9) is used to determine the strain energy density. Formula (2.20) is then applied to derive the strain energy cumulated in beam portion B_3B_4 by replacing u_{02}^* with the strain energy density u_{02}.

Finally, by substituting w and U in formula (2.24), and expressing the boundaries of integration σ_{sr} and σ_{uc}, one derives the following solution for the strain energy release rate:

$$G = \frac{F}{b}\frac{l_1 - a}{2}(\kappa_1 - \kappa_2) - \int_{-\sigma_{sr}}^{\sigma_{sr}} u_{01}\,\mathrm{d}z_1 + \int_{-\sigma_{uc}}^{\sigma_{uc}} u_{02}\,\mathrm{d}z_2, \tag{2.30}$$

where κ_1, σ_{sr}, κ_2 and σ_{uc} are obtained by Eqs. (2.18) and (2.19) at $x = l_1 + a$. The MATLAB computer program is used to perform the integration in (2.30). It should be noted that the strain energy release rate obtained by (2.30) matches that found by using (2.22). This fact serves as a verification of the solution for the strain energy release rate derived in this section of the paper.

3. Beam with asymmetrical creep behaviour in tension and compression

The strain energy release rate for the lengthwise crack in the beam configuration shown in Fig. 1 is also obtained for the case when the material exhibits asymmetrical creep behaviour in tension and compression. For this purpose, the creep in tension and compression is described by the following non-linear stress-strain-time relationships:

$$\varepsilon = A_{0t}\sinh(\beta_{0t}\sigma_t) + A_t^{n_t} t^{n_t}\sinh(\beta_t\sigma_t), \tag{3.1}$$

$$\varepsilon = A_{0c}\sinh(\beta_{0c}\sigma_c) + A_c^{n_c} t^{n_c}\sinh(\beta_c\sigma_c), \tag{3.2}$$

where σ_t and σ_c are the normal stresses, respectively, in tension and compression, t is the time, A_{0t}, β_{0t}, A_t, β_t, and n_t are material constants in tension. The material constants in compression are denoted by A_{0c}, β_{0c}, A_c, β_c, and n_c. Since the material is inhomogeneous, A_{0t}, A_t, A_{0c}, and A_c vary continuously along the beam length according to the following laws:

$$\begin{aligned} A_{0t} &= A_{0tKR}e^{\varphi_{0t}\frac{x}{l}}, \qquad A_t = A_{tKR}e^{\varphi_t\frac{x}{l}}, \\ A_{0c} &= A_{0cKR}e^{\varphi_{0c}\frac{x}{l}}, \qquad A_c = A_{cKR}e^{\varphi_c\frac{x}{l}}, \end{aligned} \tag{3.3}$$

where A_{0tKR}, A_{tKR}, A_{0cKR}, and A_{cKR} are the values of A_{0t}, A_t, A_{0c}, and A_c at the left-hand end of the beam, and φ_{0t}, φ_t, φ_{0c}, and φ_c are material constants.

It should be noted that stress-strain-time relationships (3.1)–(3.3) are used here to illustrate how to apply the analysis when the beam exhibits asymmetrical creep behaviour in tension and compression (other stress-strain-time relationships can also be used in a similar manner depending on the particular problem under consideration).

A solution for the strain energy release rate is derived by applying formula (2.3). The complementary strain energies in the compression and the tension zones in the upper crack arm are written, respectively, as:

$$U_{1c}^{*} = b \int_{l_1}^{l_1+a} \int_{-\frac{h_1}{2}}^{z_{1n}} u_{01c}^{*} \,\mathrm{d}x \,\mathrm{d}z_1 \tag{3.4}$$

and

$$U_{1t}^{*} = b \int_{l_1}^{l_1+a} \int_{z_{1n}}^{\frac{h_1}{2}} u_{01t}^{*} \,\mathrm{d}x \,\mathrm{d}z_1, \tag{3.5}$$

where u_{01c}^{*} and u_{01t}^{*} are the complementary strain energy densities in the compression and tension zones, respectively, and z_{1n} is the coordinate of the neutral axis (Fig. 2). It should be noted that the neutral axis shifts from the centroid since the material has asymmetrical creep behaviour in tension and compression. In formulas (3.4) and (3.5), it is taken into account that the upper fibres are loaded in compression in the beam under consideration. The complementary strain energy densities in the compression and tension zones are expressed, respectively, as:

$$u_{01c}^{*} = \frac{A_{0c}}{\beta_{0c}} \cosh\left(\beta_{0c}\sigma_c\right) + \frac{A_c^{n_c}}{\beta_c} t^{n_c} \cosh\left(\beta_c \sigma_c\right) \tag{3.6}$$

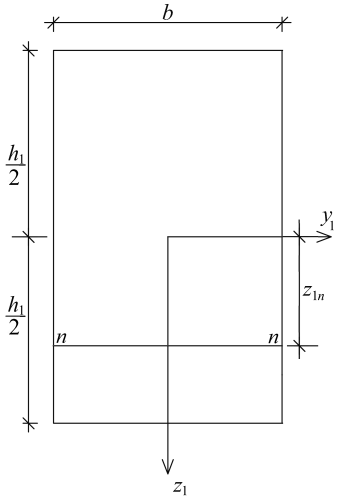

FIG. 2. Cross-section of the upper crack arm
(the position of the neutral axis is marked by $n - n$).

and

$$u^{*}_{01t} = \frac{A_{0t}}{\beta_{0t}} \cosh\left(\beta_{0t}\sigma_t\right) + \frac{A_t^{n_t}}{\beta_t} t^{n_t} \cosh\left(\beta_t \sigma_t\right). \tag{3.7}$$

The distribution of strains along the thickness of the upper crack arm is written as:

$$\varepsilon = \kappa_1 (z_1 - z_{1n}), \tag{3.8}$$

where z_{1n} is the coordinate of the neutral axis (it should be noted that the neutral axis shifts from the centroid since the material exhibits asymmetrical behaviour in tension and compression). The curvature and the coordinate of the neutral axis are determined in the following manner. First, the equations for the equilibrium of the cross-section of the upper crack arm are written as:

$$N = b \left(\int_{-\frac{h_1}{2}}^{z_{1n}} \sigma_c \, \mathrm{d}z_1 \right)_{\text{in compression zone}} + b \left(\int_{z_{1n}}^{\frac{h_1}{2}} \sigma_t \, \mathrm{d}z_1 \right)_{\text{in tension zone}}, \tag{3.9}$$

$$M = b \left(\int_{-\frac{h_1}{2}}^{z_{1n}} \sigma_c z_1 \, \mathrm{d}z_1 \right)_{\text{in compression zone}} + b \left(\int_{z_{1n}}^{\frac{h_1}{2}} \sigma_t z_1 \, \mathrm{d}z_1 \right)_{\text{in tension zone}}, \tag{3.10}$$

where N is the axial force (apparently, $N = 0$). By substituting (3.8) into (3.1), one obtains

$$\kappa_1 \left(z_1 - z_{1n}\right) = A_{0t} \sinh\left(\beta_{0t}\sigma_t\right) + A_t^{n_t} t^{n_t} \sinh\left(\beta_t \sigma_t\right). \tag{3.11}$$

For z_1 and $\mathrm{d}z_1$ in the tension zone, from (3.11) one derives:

$$z_1 = \frac{1}{\kappa_1} \left[A_{0t} \sinh\left(\beta_{0t}\sigma_t\right) + A_t^{n_t} t^{n_t} \sinh\left(\beta_t \sigma_t\right)\right] + z_{1n}, \tag{3.12}$$

$$\mathrm{d}z_1 = \frac{1}{\kappa_1} \left[A_{0t}\beta_{0t} \cosh\left(\beta_{0t}\sigma_t\right) + A_t^{n_t}\beta_t t^{n_t} \cosh\left(\beta_t \sigma_t\right)\right] \mathrm{d}\sigma_t. \tag{3.13}$$

Analogously after substituting (3.8) into (3.3), one obtains the following expressions for z_1 and $\mathrm{d}z_1$ in the compression zone:

$$z_1 = \frac{1}{\kappa_1} \left[A_{0c} \sinh\left(\beta_{0c}\sigma_c\right) + A_c^{n_c} t^{n_c} \sinh\left(\beta_c \sigma_c\right)\right] - z_{1n}, \tag{3.14}$$

$$\mathrm{d}z_1 = \frac{1}{\kappa_1} \left[A_{0c}\beta_{0c} \cosh\left(\beta_{0c}\sigma_c\right) + A_c^{n_c}\beta_c t^{n_c} \cosh\left(\beta_c \sigma_c\right)\right] \mathrm{d}\sigma_c. \tag{3.15}$$

By substituting (3.12) and (3.13) in the tension zone and (3.14) and (3.15) in the compression zone into (3.9) and (3.10) and integrating from σ_{srup} to 0 in the compression zone and from 0 to σ_{srlo} in the tension zone, one obtains

$$
\begin{aligned}
(3.16)\quad N = {} & \frac{b}{\kappa_1}\left\{A_{0c}\left[-\sigma_{srup}\sinh\left(-\beta_{0c}\sigma_{srup}\right)\right] - \frac{1}{\beta_{0c}}\left[1-\cosh\left(\beta_{0c}\sigma_{srup}\right)\right]\right\} \\
& + \frac{b}{\kappa_1}\left\{A_c^{n_c}t^{n_c}\left[-\sigma_{srup}\sinh\left(-\beta_c\sigma_{srup}\right)\right] - \frac{1}{\beta_c}\left[1-\cosh\left(\beta_c\sigma_{srup}\right)\right]\right\} \\
& + \frac{b}{\kappa_1}\left\{A_{0t}\left[\sigma_{srlo}\sinh\left(\beta_{0t}\sigma_{srlo}\right)\right] - \frac{1}{\beta_{0t}}\left[\cosh\left(\beta_{0t}\sigma_{srlo}\right)-1\right]\right\} \\
& + \frac{b}{\kappa_1}\left\{A_t^{n_t}t^{n_t}\left[\sigma_{srlo}\sinh\left(\beta_t\sigma_{srlo}\right)\right] - \frac{1}{\beta_t}\left[\cosh\left(\beta_c\sigma_{srlo}\right)-1\right]\right\},
\end{aligned}
$$

$$
\begin{aligned}
(3.17)\quad M = {} & A_{0c}^2\frac{b}{4\kappa_1^2}\left[-\sigma_{srup}\cosh\left(2\beta_{0c}\sigma_{srup}\right) + \frac{1}{2\beta_{0c}}\sinh\left(2\beta_{0c}\sigma_{srup}\right)\right] \\
& + A_c^{n_c}A_{0c}t^{n_c}\frac{b}{2\kappa_1^2}\left\{-\sigma_{srup}\cosh\left[\left(\beta_{0c}+\beta_c\right)\sigma_{srup}\right]\right. \\
& \left. + \frac{1}{\beta_c+\beta_{0c}}\sinh\left[\left(\beta_{0c}+\beta_c\right)\sigma_{srup}\right]\right\} \\
& + A_c^{n_c}A_{0c}\beta_c t^{n_c}\frac{b}{2\kappa_1^2}\left\{-\frac{1}{\beta_{0c}-\beta_c}\sigma_{srup}\cosh\left[\left(\beta_{0c}-\beta_c\right)\sigma_{srup}\right]\right. \\
& \left. + \frac{1}{\left(\beta_{0c}-\beta_c\right)^2}\sinh\left[\left(\beta_{0c}-\beta_c\right)\sigma_{srup}\right]\right\} \\
& + A_c^{n_c}A_{0c}\beta_{0c}t^{n_c}\frac{b}{2\kappa_1^2}\left\{-\frac{1}{\beta_c-\beta_{0c}}\sigma_{srup}\cosh\left[\left(\beta_c-\beta_{0c}\right)\sigma_{srup}\right]\right. \\
& \left. + \frac{1}{\left(\beta_c-\beta_{0c}\right)^2}\sinh\left[\left(\beta_c-\beta_{0c}\right)\sigma_{sr}\right]\right\} \\
& + A_c^{2n_c}t^{2n_c}\frac{b}{4\kappa_1^2}\left[-\sigma_{srup}\cosh\left(2\beta_c\sigma_{srup}\right) + \frac{1}{2\beta_c}\sinh\left(2\beta_c\sigma_{srup}\right)\right] \\
& + \frac{z_{1n}b}{\kappa_1}\left\{A_{0c}\left[-\sigma_{srup}\sinh\left(\beta_{0c}\sigma_{srup}\right) + \frac{1}{\beta_{0c}}\cosh\left(\beta_{0c}\sigma_{srup}\right) - \frac{1}{\beta_{0c}}\right]\right. \\
& \left. + A_c^{n_c}t^{n_c}\left[-\sigma_{srup}\sinh\left(\beta_c\sigma_{srup}\right) + \frac{1}{\beta_c}\cosh\left(\beta_c\sigma_{srup}\right) - \frac{1}{\beta_c}\right]\right\}
\end{aligned}
$$

$$
\begin{aligned}
(3.17)_{[\text{Cont.}]} \qquad & + A_{0t}^2 \frac{b}{4\kappa_1^2} \left[\sigma_{srlo} \cosh\left(2\beta_{0t}\sigma_{srlo}\right) - \frac{1}{2\beta_{0t}} \sinh\left(2\beta_{0t}\sigma_{srlo}\right) \right] \\
& + A_t^{n_t} A_{0t} t^{n_t} \frac{b}{2\kappa_1^2} \left\{ \sigma_{srlo} \cosh\left[\left(\beta_{0t}+\beta_t\right)\sigma_{srlo}\right] \right. \\
& \left. - \frac{1}{\beta_t+\beta_{0t}} \sinh\left[\left(\beta_{0t}+\beta_t\right)\sigma_{srlo}\right] \right\} \\
& + A_t^{n_t} A_{0t} \beta_t t^{n_t} \frac{b}{2\kappa_1^2} \left\{ \frac{1}{\beta_{0t}-\beta_t} \sigma_{srlo} \cosh\left[\left(\beta_{0t}-\beta_t\right)\sigma_{srlo}\right] \right. \\
& \left. - \frac{1}{\left(\beta_{0t}-\beta_t\right)^2} \sinh\left[\left(\beta_{0t}-\beta_t\right)\sigma_{srlo}\right] \right\} \\
& + A_t^{n_t} A_{0t} \beta_{0t} t^{n_t} \frac{b}{2\kappa_1^2} \left\{ \frac{1}{\beta_t-\beta_{0t}} \sigma_{srlo} \cosh\left[\left(\beta_t-\beta_{0t}\right)\sigma_{srlo}\right] \right. \\
& \left. - \frac{1}{\left(\beta_t-\beta_{0t}\right)^2} \sinh\left[\left(\beta_t-\beta_{0t}\right)\sigma_{srlo}\right] \right\} \\
& + A_t^{2n_t} t^{2n_t} \frac{b}{4\kappa_1^2} \left[\sigma_{srlo} \cosh\left(2\beta_t\sigma_{srlo}\right) - \frac{1}{2\beta_t} \sinh\left(2\beta_t\sigma_{srlo}\right) \right] \\
& + \frac{z_{1n} b}{\kappa_1} \left\{ A_{0t} \left[\sigma_{srlo} \sinh\left(\beta_{0t}\sigma_{srlo}\right) - \frac{1}{\beta_{0t}} \cosh\left(\beta_{0t}\sigma_{srlo}\right) + \frac{1}{\beta_{0t}} \right] \right. \\
& \left. + A_t^{n_t} t^{n_t} \left[\sigma_{srlo} \sinh\left(\beta_t\sigma_{srlo}\right) - \frac{1}{\beta_t} \cosh\left(\beta_t\sigma_{srlo}\right) + \frac{1}{\beta_t} \right] \right\},
\end{aligned}
$$

where σ_{srup} and σ_{srlo} are the normal stresses at the upper and lower surfaces of the upper crack arm, respectively. Further, two equations are written by using (3.1), (3.2), and (3.8):

$$
\kappa_1 \left(\frac{h_1}{2} - z_{1n} \right) = A_{0t} \sinh\left(\beta_{0t}\sigma_{srlo}\right) + A_t^{n_t} t^{n_t} \sinh\left(\beta_t\sigma_{srlo}\right), \tag{3.18}
$$

$$
\kappa_1 \left(-\frac{h_1}{2} - z_{1n} \right) = A_{0c} \sinh\left(\beta_{0c}\sigma_{srup}\right) + A_c^{n_c} t^{n_c} \sinh\left(\beta_c\sigma_{srup}\right). \tag{3.19}
$$

Equations (3.16)–(3.19) are solved with respect to κ_1, z_{1n}, σ_{srup}, and σ_{srlo} by using the MATLAB computer program.

The complementary strain energies in the compression and tension zones of the beam portion B_3B_4 are written, respectively, as:

$$
U_{2c}^* = b \int_{l_1+a}^{\frac{l}{2}} \int_{-\frac{h}{2}}^{z_{2n}} u_{02c}^* \, \mathrm{d}x \, \mathrm{d}z_2 \tag{3.20}
$$

and

$$U_{2t}^{*} = b \int_{l_1+a}^{\frac{l}{2}} \int_{z_{2n}}^{\frac{h}{2}} u_{02t}^{*} \, \mathrm{d}x \, \mathrm{d}z_2. \tag{3.21}$$

By replacing κ_1 with κ_2 in (3.13), one obtains the following expression for $\mathrm{d}z_2$ in the tension zone of the beam portion B_3B_4:

$$\mathrm{d}z_2 = \frac{1}{\kappa_2} \left[A_{0t}\beta_{0t} \cosh\left(\beta_t \sigma_t\right) + A_t^{n_t} \beta_t t^{n_t} \cosh\left(\beta_t \sigma_t\right) \right] \mathrm{d}\sigma_t. \tag{3.22}$$

The quantity $\mathrm{d}z_2$ in the compression zone of the beam portion B_3B_4 is found by replacing κ_1 with κ_2 in (3.15):

$$\mathrm{d}z_2 = \frac{1}{\kappa_2} \left[A_{0c}\beta_{0c} \cosh\left(\beta_{0c} \sigma_c\right) + A_c^{n_c} \beta_c t^{n_c} \cosh\left(\beta_c \sigma_c\right) \right] \mathrm{d}\sigma_c. \tag{3.23}$$

Equations (3.15)–(3.19) are used to determine the unknowns κ_2, z_{2n}, σ_{ucup}, and σ_{uclo}, where z_{2n} is the coordinate of the neutral axis, σ_{ucup} and σ_{uclo} are the normal stresses, respectively, at the upper and lower surface of the beam in the portion B_3B_4. For this purpose, h_1, κ_1, z_{1n}, σ_{srup}, and σ_{srlo} are replaced, respectively, with h, κ_2, z_{2n}, σ_{ucup}, and σ_{uclo}.

The complementary strain energy involved in (2.3) is written as:

$$U^{*} = U_{1c}^{*} + U_{1t}^{*} + U_{2c}^{*} + U_{2t}^{*}. \tag{3.24}$$

By substituting (3.4), (3.5), (3.20), (3.21) and (3.24) into (2.3) and expressing the boundaries of integration through the stresses, σ_{srup}, σ_{srlo}, σ_{ucup}, and σ_{uclo}, one obtains:

$$G = \int_{\sigma_{srup}}^{0} u_{01c}^{*} \, \mathrm{d}z_1 + \int_{0}^{\sigma_{srlo}} u_{01t}^{*} \, \mathrm{d}z_1 - \int_{\sigma_{ucup}}^{0} u_{02c}^{*} \, \mathrm{d}z_2 - \int_{0}^{\sigma_{uclo}} u_{02t}^{*} \, \mathrm{d}z_2, \tag{3.25}$$

where formulas (3.22) and (3.23) are used to obtain $\mathrm{d}z_1$ in tension and compression, respectively, and formulas (3.22) and (3.23) are used to obtain $\mathrm{d}z_2$ in tension and compression zones, respectively. The quantitiesκ_1, z_{1n}, σ_{srup}, σ_{srlo}, κ_2, z_{2n}, σ_{ucup}, and σ_{uclo} are determined by (3.16)–(3.19) at $x = l_1 + a$. The integration in (3.25) is performed by the MATLAB computer program.

The time-dependent strain energy release rate is also derived by considering the balance of energy in order to verify (3.25). For this purpose, formula (2.25) is applied. The vertical displacement of the application point of the external

force F is determined by using expression (2.29) where, in this case, the curvatures are determined by Eqs. (3.16)–(3.19). The strain energy involved in (2.28) is written as:

$$U = U_{1c} + U_{1t} + U_{2c} + U_{2t}, \tag{3.26}$$

where U_{1c} and U_{1t} are, respectively, the strain energies in the compression and tension zones of the upper crack arm, and U_{2c} and U_{2t} are the strain energies, respectively, in the compression and tension zones of the beam portion B_3B_4.

The strain energies in the compression and tension zones of the upper crack arm are found, respectively, as:

$$U_{1c} = b \int_{l_1}^{l_1+a} \int_{-\frac{h_1}{2}}^{z_{1n}} u_{01c}\,\mathrm{d}x\,\mathrm{d}z_1 \tag{3.27}$$

and

$$U_{1t} = b \int_{l_1}^{l_1+a} \int_{z_{1n}}^{\frac{h_1}{2}} u_{01t}\,\mathrm{d}x\,\mathrm{d}z_1. \tag{3.28}$$

By using formula (2.9), the strain energy densities in the compression and tension zones involved in (3.27) and (3.28) are obtained, respectively, as:

$$u_{01c} = A_{0c}\left[\sigma_c \sinh(\beta_{0c}\sigma_c) - \frac{1}{\beta_{0c}}\cosh(\beta_{0c}\sigma_c)\right] + A_c^{n_c} t^{n_c}\left[\sigma_c \sinh(\beta_c\sigma_c) - \frac{1}{\beta_c}\cosh(\beta_c\sigma_c)\right] \tag{3.29}$$

and

$$u_{01t} = A_{0t}\left[\sigma_t \sinh(\beta_{0t}\sigma_t) - \frac{1}{\beta_{0t}}\cosh(\beta_{0t}\sigma_t)\right] + A_t^{n_t} t^{n_t}\left[\sigma_t \sinh(\beta_t\sigma_t) - \frac{1}{\beta_t}\cosh(\beta_t\sigma_t)\right]. \tag{3.30}$$

The strain energies cumulated in the compression and tension zones of the beam portion, B_3B_4 are written, respectively, as:

$$U_{2c} = b \int_{l_1+a}^{\frac{l}{2}} \int_{-\frac{h}{2}}^{z_{2n}} u_{02c}\,\mathrm{d}x\,\mathrm{d}z_2 \tag{3.31}$$

and

$$U_{2t} = b \int\limits_{l_1+a}^{\frac{l}{2}} \int\limits_{z_{2n}}^{\frac{h}{2}} u_{02t} \, \mathrm{d}x \, \mathrm{d}z_2. \tag{3.32}$$

By substituting (2.28), (3.26), (3.27), (3.28), (3.31), and (3.32) into (2.24) and expressing the boundaries of integration through the stresses σ_{srup}, σ_{srlo}, σ_{ucup}, and σ_{uclo}, one obtains the following solution of the strain energy release rate:

$$G = \frac{F}{b} \frac{l_1 - a}{2} (\kappa_1 - \kappa_2) - \int\limits_{\sigma_{srup}}^{0} u_{01c} \, \mathrm{d}z_1 - \int\limits_{0}^{\sigma_{srlo}} u_{01t} \, \mathrm{d}z_1 + \int\limits_{\sigma_{ucup}}^{0} u_{02c} \, \mathrm{d}z_2 \int\limits_{0}^{\sigma_{uclo}} u_{02t} \, \mathrm{d}z_2, \tag{3.33}$$

where κ_1, z_{1n}, σ_{srup}, σ_{srlo}, κ_2, z_{2n}, σ_{ucup}, and σ_{uclo}, are determined by (3.16)–(3.19) at $x = l_1 + a$. The integration in (3.33) is performed by using the MATLAB computer program. The strain energy release rate found by (3.33) matches that obtained by (3.25), which is a verification of the analysis for the case when the material exhibits asymmetrical creep behaviour in tension and compression.

It should be mentioned that the solutions (2.22), (2.3), (3.25), and (3.33) are time-dependent since the strain energy densities are continuous functions of time due to the creep (refer to formulas (2.9) and (2.10)). Therefore, these solutions can be applied to evaluate the creep-induced continuous change in the strain energy release rate with time.

4. Numerical results

This section presents the results obtained by applying the solutions of the strain energy release rate derived in the previous Sections 2 and 3. The strain energy release rate is expressed in non-dimensional form by using the formula $G_N = G\beta_0/b$. The changes in the strain energy release rate over time, as well as the influence of the crack's location along the thickness of the beam, crack length, bending moment value, and ratios of material properties in tension and compression are investigated. It is assumed that $b = 0.0020$ m, $h = 0.004$ m, $l = 0.130$ m and $F = 4$ N. For a beam that exhibits identical creep behaviour in tension and compression, it is assumed that $A_{0KR} = 0.0015$, $\beta_0 = 0.1 \cdot 10^{-7}$ Pa^{-1}, $\varphi_0 = 0.4$, $\varphi = 0.4$, and $n = 0.0012$ (the remaining parameters are varied for the purpose

of the parametric analysis). It should be noted that in the case of asymmetrical creep behaviour, the parameters in tension are chosen to be 30% higher compared to the values in the symmetrical case. Additionally, the parameters in compression are varied for the purpose of the parametric analysis. It should be underlined that the parameters used in the present study are mainly for illustrative purposes. Other parameters can also be used depending on the particular problem.

First, the change in strain energy release rate over time induced by non-linear creep is analysed at different locations of the crack along the beam thickness. For this purpose, the time-dependent solution for strain energy release rate, derived for the case where the material exhibits identical creep behaviour in tension and compression, is applied. Calculations of the strain energy release rate are performed at the various time values for three h_1/h ratios. One can get an idea about the change of strain energy release rate over time in Fig. 3 where the strain energy release rate in non-dimensional form is plotted against the non-dimensional time for three h_1/h ratios. The increase in strain energy release rate over time, which can be observed in Fig. 3, is induced by the non-linear creep. One can observe also in Fig. 3 that the strain energy release rate decreases with increasing h_1/h ratio.

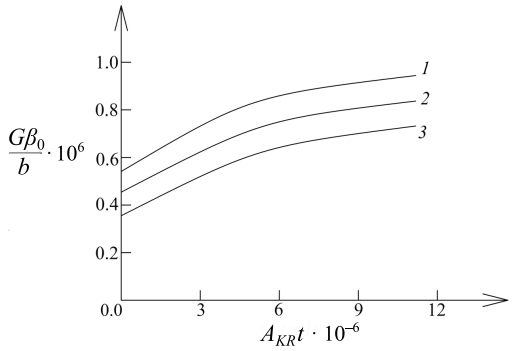

FIG. 3. The non-dimensional strain energy release rate for identical creep behaviour in tension and compression plotted against the non-dimensional time (curve 1 – at $h_1/h = 0.2$, curve 2 – at $h_1/h = 0.4$, and curve 3 – at $h_1/h = 0.6$).

The change of the strain energy release rate over time is investigated also for the case where the material has asymmetrical creep behaviour in tension and compression. The effect of crack length is investigated too (the crack length is characterised by a/l ratio). The results of the calculations are illustrated in Fig. 4 where the strain energy release rate in non-dimensional form is plotted against the non-dimensional time at three a/l ratios. The curves in Fig. 4 indicate that the strain energy release rate increases over time.

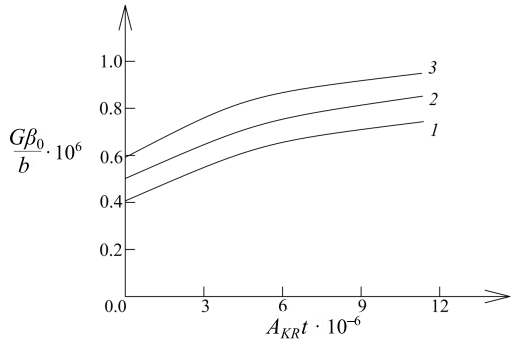

FIG. 4. The non-dimensional strain energy release rate for asymmetrical creep behaviour in tension and compression plotted against the non-dimensional time (curve 1 – at $a/l = 0.2$, curve 2 – at $a/l = 0.3$, and curve 3 – at $a/l = 0.4$).

The influence of the external force value on the strain energy release rate is analysed. For this purpose, calculations are carried out at different external force F values by applying the solutions of the strain energy release rate (2.22) and (3.25). The strain energy release rates obtained from (2.22) and (3.25) are plotted against the force value in Fig. 5. The curves in Fig. 5 demonstrate that the strain energy release rate increases with an increase in force. It can also be observed in Fig. 5 that the strain energy release rate for the case when the material has identical creep behaviour in tension and compression is lower than that for the case when the material has asymmetrical creep behaviour.

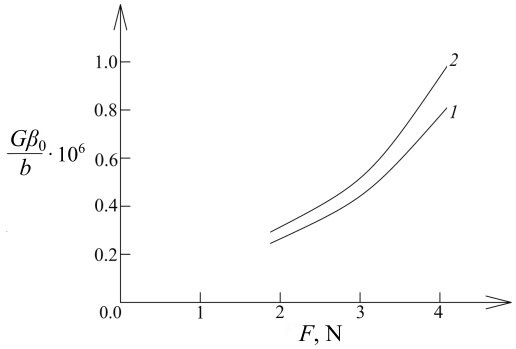

FIG. 5. The non-dimensional strain energy release rate plotted against the value of the force F (curve 1 – at identical creep behaviour in tension and compression, curve 2 – at asymmetrical creep behaviour in tension and compression).

The effect of A_{KR}/A_{0KR} and β/β_0 ratios on the strain energy release rate is studied too. Calculations are performed for various A_{KR}/A_{0KR} and β/β_0 ratios by using the solution of strain energy release rate for the case when the

material has identical creep behaviour in tension and compression. The effects of A_{KR}/A_{0KR} and β/β_0 ratios are illustrated in Fig. 6 where the strain energy release rate in non-dimensional form is plotted against A_{KR}/A_{0KR} ratio for three β/β_0 ratios. One can observe in Fig. 6 that the strain energy release rate increases with increasing A_{KR}/A_{0KR} ratio. The increase of β/β_0 ratio also leads to an increase in the strain energy release rate (Fig. 6).

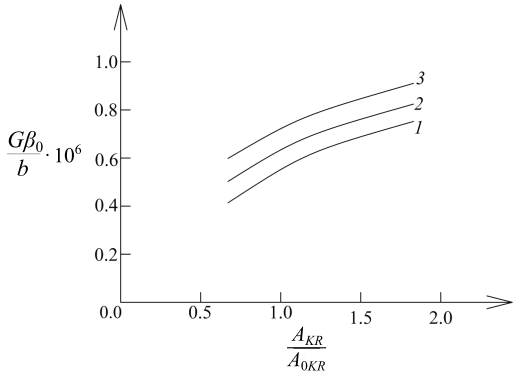

FIG. 6. The non-dimensional strain energy release rate plotted against A_{KR}/A_{0KR} ratio (curve 1 – at $\beta/\beta_0 = 0.5$, curve 2 – at $\beta/\beta_0 = 1$, and curve 3 – at $\beta/\beta_0 = 2$).

The effect of the asymmetric creep behaviour of the material in tension and compression is also evaluated. For this purpose, first, calculations of the strain energy release rate are performed at various A_{0cKR}/A_{0tKR} and β_{0c}/β_{0t} ratios. The strain energy release rate in non-dimensional form is plotted against A_{0cKR}/A_{0tKR} ratio at three β_{0c}/β_{0t} ratios in Fig. 7. The curves in Fig. 7 indicate that the strain energy release rate increases with increasing A_{0cKR}/A_{0tKR} ratio.

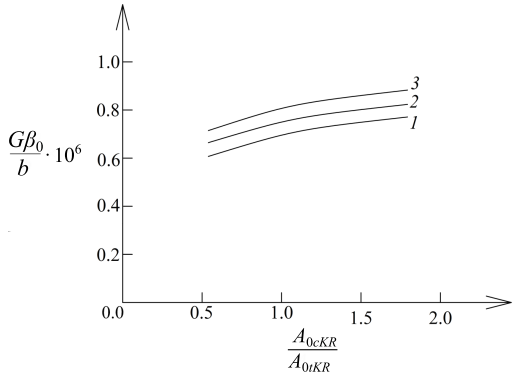

FIG. 7. The non-dimensional strain energy release rate plotted against A_{0cKR}/A_{0tKR} ratio (curve 1 – at $\beta_{0c}/\beta_{0t} = 0.5$, curve 2 – at $\beta_{0c}/\beta_{0t} = 1$, and curve 3 – at $\beta_{0c}/\beta_{0t} = 2$).

One can also observe in Fig. 7 that the strain energy release rate increases with increasing β_{0c}/β_{0t} ratio.

The effects of A_{cKR}/A_{tKR} and β_c/β_t ratios on the strain energy release rate are displayed in Fig. 8 where the strain energy release rate in non-dimensional form is plotted against A_{cKR}/A_{tKR} ratio at three β_c/β_t ratios. The curves in Fig. 8 demonstrate that the strain energy release rate increases with an increase in A_{cKR}/A_{tKR} and β_c/β_t ratios.

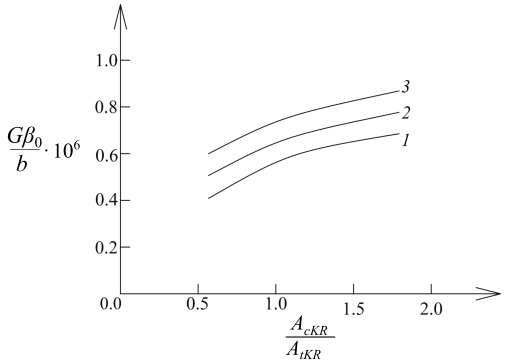

FIG. 8. The non-dimensional strain energy release rate plotted against A_{cKR}/A_{tKR} ratio (curve 1 – at $\beta_c/\beta_t = 0.5$, curve 2 – at $\beta_c/\beta_t = 1$, and curve 3 – at $\beta_c/\beta_t = 2$).

Variation of the non-dimensional strain energy release rate with increasing φ_{0t} and φ_t is depicted in Fig. 9. It can be observed that the strain energy release rate reduces when φ_{0t} and φ_t increase (Fig. 9).

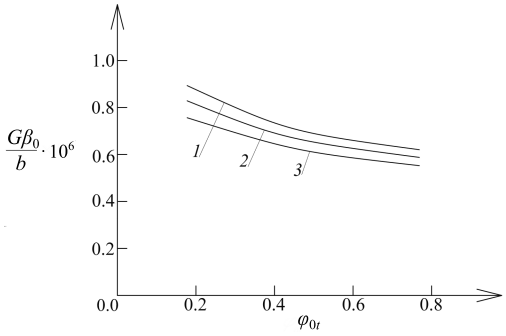

FIG. 9. The non-dimensional strain energy release rate plotted against φ_{0t} (curve 1 – at $\varphi_t = 0.3$, curve 2 – at $\varphi_t = 0.6$, and curve 3 – at $\varphi_t = 0.9$).

5. Conclusion

The strain energy release rate for a lengthwise crack in a beam configuration that exhibits non-linear creep behaviour was studied analytically. The material

was continuously inhomogeneous along the beam length. The beam was loaded in three-point bending by a vertical force applied in the mid-span. The lengthwise crack was arbitrarily located along the thickness of the beam cross-section. Two cases (a beam with identical creep behaviour in tension and compression and a beam with asymmetrical creep behaviour) were analysed. Time-dependent solutions of the strain energy release rate were derived for the two cases under consideration. For this purpose, the time-dependent complementary strain energy cumulated in the beam was analysed. The creep behaviour of the material was described using a non-linear stress-strain-time relationship. Since the stress cannot be determined explicitly from the non-linear stress-strain-time relationship, an approach for analysis of the strain energy release rate was developed by expressing the z-coordinate through the stress.

The time-dependent solutions of strain energy release rate were verified by analysing the energy balance in the beam. These solutions were applied to evaluate the change in strain energy release rate over time. The analysis revealed that the creep induced increase of the strain energy release rate overtime. It was found that the strain energy release rate in the beam with asymmetrical creep behaviour in tension and compression was higher than that in the beam with identical creep behaviour. The analysis also revealed that the strain energy release rate increased with increasing the crack length. The increase of h_1/h ratio induced a decrease in strain energy release rate. It was also found that the strain energy release rate increases with increasing A_{KR}/A_{0KR} ratio. The investigation showed that the increase of β/β_0 ratio generated an increase in strain energy release rate.

In order to evaluate the effects of the asymmetrical creep behaviour of the material in tension and compression on the strain energy release rate, calculations were conducted for various A_{0cKR}/A_{0tKR}, β_{0c}/β_{0t}, A_{cKR}/A_{tKR}, and β_c/β_t ratios. The analysis indicated that the strain energy release rate increased with increasing A_{0cKR}/A_{0tKR}, β_{0c}/β_{0t}, A_{cKR}/A_{tKR}, and β_c/β_t ratios. This finding suggests that the asymmetrical creep behaviour of the material induces an increase of the strain energy release rate. Therefore, asymmetrical non-linear creep behaviour is crucial in fracture-mechanics-based safety design of continuously inhomogeneous structural members and components. These conclusions are valid for the selected parameters. The conclusions for other parameters (or, for instance, for other stress-strain-time relationships and other laws for distribution of the properties along the beam length) may differ to some degree. It should be underlined again that the parameters used here are mainly for illustrative purposes.

A possible practical application of the present study is determining the time value at which the lengthwise crack will begin to propagate. This can be done by analysing the non-linear creep-induced evolution of the strain energy with time

(the value of time at which the strain energy release rate falls in line with the fracture toughness is the time of beginning of the crack propagation). It should be specified further that the stress-strain-time relationships (2.1), (3.1), (3.2) and exponential laws (2.2) and (3.3) used in this study illustrate the application of the presented analysis. Other stress-strain-time relationships and laws of distribution of the properties in the beams can be used in a similar way depending on the particular lengthwise fracture problem under consideration.

References

1. Tutuncu N., Ozturk M., Exact solutions for stresses in functionally graded pressure vessels, *Composites Part B: Engineering*, **32**(8): 683–686, 2001, doi: 10.1016/S1359-8368(01)00041-5.
2. Tutuncu N., Stresses in thick-walled FGM cylinders with exponentially-varying properties, *Engineering Structures*, **29**(9): 2032–2035, 2007, doi: 10.1016/j.engstruct.2006.12.003.
3. Tutuncu N., Temel B., An efficient unified method for thermoelastic analysis of functionally graded rotating disks of variable thickness, *Mechanics of Advanced Materials and Structures*, **20**(1): 38–46, 2013, doi: 10.1080/15376494.2011.581413.
4. Arefi M., Rahimi G.H., Non linear analysis of a functionally graded beam with variable thickness, *Scientific Research and Essays*, **8**(6): 256–264, 2013, doi: 10.5897/SRE10.342.
5. Arefi M., Nonlinear analysis of a functionally graded beam resting on the elastic nonlinear foundation, *Journal of Theoretical and Applied Mechanics*, **44**(2): 71–82, 2014, doi: 10.2478/jtam-2014-0011.
6. Arefi M., Elastic solution of a curved beam made of functionally graded materials with different cross sections, *Steel and Composite Structures*, **18**(3): 659–672, 2015, doi: 10.12989/scs.2015.18.3.659.
7. Akbaş Ş.D., Nonlinear static analysis of functionally graded porous beams under thermal effect, *Coupled Systems Mechanics*, **6**(4): 399–415, 2017, doi: 10.12989/CSM.2017.6.4.399.
8. Akbaş Ş.D., Nonlinear thermal displacements of laminated composite beams, *Coupled Systems Mechanics*, **7**(6): 691–705, 2018, doi: 10.12989/CSM.2018.7.6.691.
9. Akbaş Ş.D., Hygro-thermal post-buckling analysis of a functionally graded beam, *Coupled Systems Mechanics*, **8**(5): 459–471, 2019, doi: 10.12989/CSM.2019.8.5.459.
10. Miyamoto Y., Kaysser W.A., Rabin B.H., Kawasaki A., Ford R.G., *Functionally Graded Materials: Design, Processing and Applications*, Kluwer Academic Publishers, Dordrecht/London/Boston, 1999.
11. Mahamood R.M., Akinlabi E.T., *Functionally Graded Materials*, Springer, 2017.
12. Bohidar S.K., Sharma R., Mishra P.R., Functionally graded materials: A critical review, *International Journal of Research*, **1**(7): 289–301, 2014, https://journals.pen2print.org/index.php/ijr/article/view/378.
13. Markworth A.J., Ramesh K.S., Parks Jr. W.P., Modelling studies applied to functionally graded materials, *Journal of Materials Science*, **30**(9): 2183–2193, 1995, doi: 10.1007/BF01184560.

14. Gasik M.M., Functionally graded materials: bulk processing techniques, *International Journal of Materials and Product Technology*, **39**(1–2): 20–29, 2010, doi: 10.1504/IJMPT.2010.034257.

15. Hsueh C.H., Tuan W.H., Wei W.C.J., Analyses of steady-state interface fracture of elastic multilayered beams under four-point bending, *Scripta Materialia*, **60**(8): 721–724, 2006, doi: 10.1016/j.scriptamat.2009.01.001.

16. Hutchinson J.W., Suo Z., Mixed mode cracking in layered materials, *Advances in Applied Mechanics*, **29**: 63–191, 1991, doi: 10.1016/S0065-2156(08)70164-9.

17. Carpinteri A., Pugno N., Cracks and re-entrant corners in functionally graded materials, *Engineering Fracture Mechanics*, **73**(10): 1279–1291, 2006, doi: 10.1016/j.engfracmech.2006.01.008.

18. Tilbrook M.T., Moon R.J., Hoffman M., Crack propagation in graded composites, *Composites Science and Technology*, **65**(2): 201–220, 2005, doi: 10.1016/j.compscitech.2004.07.004.

19. Yang J., Chen Y., Free vibration and buckling analyses of functionally graded beams with edge cracks, *Composite Structures*, **83**(1): 48–60, 2008, doi: 10.1016/j.compstruct.2007.03.006.

20. Rizov V.I., Statically undetermined functionally graded beam under torsion: A longitudinal fracture analysis with considering creep, *AIP Conference Proceedings*, **2557**(1): 040006-1, 2022, doi: 10.1063/5.0104158.

21. Rizov V.I., Continuously inhomogeneous beam structure with creep: a longitudinal crack study, *Structural Monitoring and Maintenance*, **8**(1): 111–124, 2021, doi: 10.12989/smm.2021.8.1.111.

22. Narisawa I., *Strength of Polymer Materials* [in Russian], Chemistry Publishing House, Moscow, 1987.

Received November 22, 2022; accepted version November 8, 2023.
Online first January 17, 2024.